# Variational multiscale stabilization for compressible flow

Margarida Moragues Ginard[a,*], Mariano Vázquez[b,c], Guillaume Houzeaux[b]

[a] *BCAM - Basque Center for Applied Mathematics, Spain*
[b] *Barcelona Supercomputing Center, Spain*
[c] *IIIA-CSIC Barcelona, Spain*

**Abstract**

This paper presents a variational multiscale stabilization for the finite element numerical solution of the Euler and Navier-Stokes equations of compressible flow. All the components of the dual operator are considered in the stabilization term and two options are proposed for the computation of the variational multiscale stabilization subscale. The first option that we call *diagonal $\tau$ subscale*, presents the classical form for the subscale as the product of a parameter $\tau$ times the residual of the equation. The second option that we call *Fourier subscale* uses the Fourier transform in order to model the subscale. We compare these two options for the variational multiscale stabilization subscale through several two-dimensional benchmark cases of different complexity in viscous and inviscid flows, covering a wide range of Mach numbers.

*Keywords:* Variational multiscale stabilization method, finite elements, compressible flow, diagonal $\tau$ subscale, Fourier subscale.

## 1. Introduction

It is well know that the straightforward finite element (FE) solution of a convection dominated problem, as for example the Euler and Navier-Stokes equations, introduces some numerical oscillations [1]. These non-physical oscillations can make the solution to blow-up, then different stabilization techniques are used to treat them. Some stabilization methods for the FE solution of compressible flows, in chronological order of appearance, are the *Streamline Upwind Petrov-Galerkin* (SUPG) [2, 3, 4, 5], the *Galerkin/Least-Squares* (GLS) [6], and the *Variational Multiscale Stabilization* (VMS) method. We can find a full survey of SUPG and GLS in [7].

*mmoragues@bcamath.org

The VMS framework was introduced in the 90's in the context of the advection-diffusion equations [8, 9] by a group of researchers lead by professor Hughes. The VMS method relies on the idea that the unknown, $\mathbf{\Phi}$, consists of two components, the large scale component, $\mathbf{\Phi}^h$, and a subscale component, $\tilde{\mathbf{\Phi}}$, to give $\mathbf{\Phi} = \mathbf{\Phi}^h + \tilde{\mathbf{\Phi}}$. The large scale is the part of the unknown that is captured by the mesh and then solved by the FE method. The subscale is the part of the unknown that is under the resolution of the mesh then cannot be solved by the numerical method. They explain that the stability problems of the FE discretization come from the fact that the effect of the subscales on the solution is not captured by the FE method. For this reason, in the VMS framework the subscales are modeled in some way, using the information that we have at the mesh scale level, and its effect is introduced in the formulation of the FE discrete problem.

VMS has been widely applied to advection-diffusion-reaction problems (e.g. [8, 9, 10, 11, 12]) as well as to the incompressible Navier-Stokes equations (e.g. [13, 14, 15, 16, 17]). Its application to compressible flow problems is more recent. As far as we know, VMS for compressible flows can be found in [18, 19] applied to two-dimensional supersonic flow problems, and in [20, 21, 22] applied to atmospheric flow. In [23, 24, 25] the proposed method is coupled to local preconditioning techniques to accelerate the convergence to the solution, specially in the low Mach and transonic regimes. Hybrid VMS-LES approaches for large eddy simulation of turbulent compressible flows can be found in [26, 27, 28, 29, 30, 31].

In this work a VMS method for the Navier-Stokes and Euler equations of compressible flow is proposed. We focus on VMS because of its robustness and validity at all Mach regimes. Also because it allows the development of new stabilization schemes as well as the understanding of previous stabilization techniques as SUPG and GLS. The Navier-Stokes equations are discretized in space by means of the FE method. An explicit method is used for the time discretization. Our VMS stabilization term takes into account the dual operator composed of all its parts. We mean by dual operator, the dual of the space differential operator, defined in Section 3.3. Concerning the VMS subscale, we consider two options: the *diagonal $\tau$ subscale* and the *Fourier subscale*. Both subscale options of the VMS method are tested and compared within a collection of two-dimensional test cases of viscous and inviscid, steady and transient flow at different Mach numbers.

The Navier-Stokes and Euler equations are set in Section 2. In Section 3 we set the basis of the FE numerical discretization and introduce the VMS method, considering the two options

mentioned above. The numerical results are presented and analyzed in Section 4. Finally, our conclusions are reported in Section 5.

## 2. Navier-Stokes equations

Let $d$ be the space dimension, which is two or three. The Navier-Stokes equations result from the conservation principles of momentum, mass, and energy. In three dimensions and conservative form they read

$$\frac{\partial \mathbf{\Phi}}{\partial t} + \frac{\partial \mathbf{F}^i(\mathbf{\Phi})}{\partial x_i} = 0 \,, \tag{1}$$

where $i = 1, \ldots, 3$ labels the space dimension. We take the Einstein summation convention that implies summation over repeated indexes in the same term. The conservative set of unknowns or conservative variables in (1) are

$$\mathbf{\Phi} = (U_1 \; U_2 \; U_3 \; \rho \; E)^{\mathrm{T}} \;, \tag{2}$$

where $U_1$, $U_2$, $U_3$ are the momentum components in the three space directions, $\rho$ is the density, and $E$ is the total energy, all them are functions of space $\mathbf{x} = (x_1, x_2, x_3)$ and time $t$. We note $\mathbf{U}$ the momentum vector, that is $\mathbf{U} = (U_1, U_2, U_3)$. The superscript $\mathrm{T}$ represents the transposed vector. Vectors $\mathbf{F}^i$ in (1) are the fluxes, which are the sum of a convective part $\mathbf{F}^{\mathrm{conv,i}}$ and a diffusive part $\mathbf{F}^{\mathrm{diff,i}}$. The convective part reads

$$\mathbf{F}^{\mathrm{conv},1} = \begin{bmatrix} \frac{U_1 U_1}{\rho} + p \\ \frac{U_2 U_1}{\rho} \\ \frac{U_3 U_1}{\rho} \\ U_1 \\ \frac{U_1}{\rho}(E+p) \end{bmatrix} \,, \quad \mathbf{F}^{\mathrm{conv},2} = \begin{bmatrix} \frac{U_1 U_2}{\rho} \\ \frac{U_2 U_2}{\rho} + p \\ \frac{U_3 U_2}{\rho} \\ U_2 \\ \frac{U_2}{\rho}(E+p) \end{bmatrix} \,, \quad \mathbf{F}^{\mathrm{conv},3} = \begin{bmatrix} \frac{U_1 U_3}{\rho} \\ \frac{U_2 U_3}{\rho} \\ \frac{U_3 U_3}{\rho} + p \\ U_3 \\ \frac{U_3}{\rho}(E+p) \end{bmatrix} \,, \tag{3}$$

where $p = \frac{R}{c_{\mathrm{v}}}(E - \frac{1}{2}\frac{U_k U_k}{\rho})$ is the pressure, $R = c_{\mathrm{p}} - c_{\mathrm{v}}$ is the constant of perfect gases, and $c_{\mathrm{p}}$ and $c_{\mathrm{v}}$ are the coefficients of specific heat at constant pressure and volume, respectively. The diffusive

part reads

$$\mathbf{F}^{\text{diff},1} = \begin{bmatrix} \tau_{11} \\ \tau_{21} \\ \tau_{31} \\ 0 \\ \frac{U_k \tau_{k1}}{\rho} - q_1 \end{bmatrix}, \quad \mathbf{F}^{\text{diff},2} = \begin{bmatrix} \tau_{12} \\ \tau_{22} \\ \tau_{32} \\ 0 \\ \frac{U_k \tau_{k2}}{\rho} - q_2 \end{bmatrix}, \quad \mathbf{F}^{\text{diff},3} = \begin{bmatrix} \tau_{13} \\ \tau_{23} \\ \tau_{33} \\ 0 \\ \frac{U_k \tau_{k3}}{\rho} - q_3 \end{bmatrix}, \tag{4}$$

where

$$\begin{aligned} \tau_{ij} &= \mu \left[ \left( \frac{\partial u_i}{\partial x_j} + \frac{\partial u_j}{\partial x_i} \right) - \delta_{ij} \frac{2}{3} \frac{\partial u_k}{\partial x_k} \right] \\ &= \frac{\mu}{\rho} \left( \frac{\partial U_i}{\partial x_j} + \frac{\partial U_j}{\partial x_i} - \frac{U_i}{\rho} \frac{\partial \rho}{\partial x_j} - \frac{U_j}{\rho} \frac{\partial \rho}{\partial x_i} \right) - \delta_{ij} \frac{2}{3} \frac{\mu}{\rho} \left( \frac{\partial U_k}{\partial x_k} - \frac{U_k}{\rho} \frac{\partial \rho}{\partial x_k} \right) \end{aligned} \tag{5}$$

and

$$q_j = -\kappa \frac{\partial T}{\partial x_j} = -\frac{\kappa}{c_{\text{v}} \rho} \left[ \left( \frac{U_k U_k}{\rho^2} - \frac{E}{\rho} \frac{\partial \rho}{\partial x_j} \right) - \frac{U_k}{\rho} \frac{\partial U_k}{\partial x_j} + \frac{\partial E}{\partial x_j} \right], \tag{6}$$

for $i, j = 1, \ldots, 3$, are the deviatoric stress tensor and the heat flux, respectively. In (5)-(6), $\mu$ is the viscosity, and $\kappa$ is the coefficient of heat conductivity. $\mu$ and $\kappa$ are supposed constant unless is otherwise specified.

Other important physical variables and quantities are: the velocity $\mathbf{u} = \frac{\mathbf{U}}{\rho}$, the total energy per unit mass $e = \frac{E}{\rho}$, the internal energy per unit mass $i = e - \frac{1}{2}\|\mathbf{u}\|^2$, the temperature $T = i/c_v = \frac{1}{c_{\text{v}}\rho}(E - \frac{1}{2}\frac{U_k U_k}{\rho})$, the Mach number $M = \frac{\|\mathbf{u}\|}{c}$, the speed of the sound $c = \sqrt{\gamma \frac{p}{\rho}}$, and the specific heat ratio $\gamma = \frac{c_{\text{p}}}{c_{\text{v}}}$. The pressure and the temperature can be related by the expression $p = \rho R T$. In this work $\|\cdot\|$ represents the $L^2$ norm. It is also useful to define the Prandtl number $Pr = \frac{c_{\text{p}}\,\mu}{\kappa}$ and the Reynolds number $Re = \frac{\rho_{\text{ch}}\,\|\mathbf{u}_{\text{ch}}\|\,L}{\mu}$, where $\rho_{\text{ch}}$, $L$, and $\mathbf{u}_{\text{ch}}$ are, respectively, a characteristic density, length, and velocity of the problem.

The three-dimensional Navier-Stokes equations (1) can be re-written in non-conservative form as follows:

$$\frac{\partial \mathbf{\Phi}}{\partial t} + \mathbf{A}^i(\mathbf{\Phi}) \frac{\partial \mathbf{\Phi}}{\partial x_i} - \frac{\partial}{\partial x_i} \left( \mathbf{K}^{ir}(\mathbf{\Phi}) \frac{\partial \mathbf{\Phi}}{\partial x_r} \right) = 0, \tag{7}$$

for $i, r = 1, \ldots, 3$, where $\mathbf{\Phi}$ is the vector of the conservative set of unknowns (2), $\mathbf{A}^i(\mathbf{\Phi}) = \frac{\partial \mathbf{F}^i}{\partial \mathbf{\Phi}}$ are the Euler jacobian matrices and $\mathbf{K}^{ir}$ are the diffusion matrices such that $\mathbf{F}^{\text{diff,i}} = \mathbf{K}^{ir} \frac{\partial \mathbf{\Phi}}{\partial x_r}$. $\mathbf{A}^i$ and $\mathbf{K}^{ir}$ are $(d+2) \times (d+2)$ matrices whose explicit expressions in three dimensions can be found in Appendix A. Given a bounded domain $\Omega \subset \mathbb{R}^3$, and a time interval $(0, T)$, $T \in \mathbb{R}$, $T > 0$, the

problem is to find $\mathbf{\Phi}(\mathbf{x}, t)$ satisfying equation (7) with proper initial and boundary conditions, for all $(\mathbf{x}, t) \in \Omega \times (0, T)$. Boundary and initial conditions depend on the problem under study.

The Euler equations are the inviscid equations of compressible flow. They are a particular case of the Navier-Stokes equations (7) for which the viscosity is assumed to be zero, that is $\mu = 0$. Thus the three-dimensional Euler equations can be written in non-conservative form as follows:

$$\frac{\partial \mathbf{\Phi}}{\partial t} + \mathbf{A}^i(\mathbf{\Phi}) \, \frac{\partial \mathbf{\Phi}}{\partial x_i} = 0 \, , \tag{8}$$

for $i = 1, \ldots, 3$.

## 3. Numerical formulation

### *3.1. Variational form*

The variational or weak form of the Navier-Stokes equations (7) is its projection on a chosen test function space $W \subset L^2(\Omega)$:

$$\int_\Omega \psi \, \frac{\partial \mathbf{\Phi}}{\partial t} \, d\Omega + \int_\Omega \psi \, \mathbf{A}^i(\mathbf{\Phi}) \, \frac{\partial \mathbf{\Phi}}{\partial x_i} \, d\Omega - \int_\Omega \psi \, \frac{\partial}{\partial x_i} \left( \mathbf{K}^{ir}(\mathbf{\Phi}) \, \frac{\partial \mathbf{\Phi}}{\partial x_r} \right) \, d\Omega = 0 \, , \tag{9}$$

for all $\psi \in W$. $L^2(\Omega)$ is the space of square-integrable real-valued functions over $\Omega$ and we take the projection by the $L^2$ scalar product. We consider $\psi$ to be a scalar function because we take the same test function $\psi$ for all the equations of our system (7). In order to relax the derivation requirements of the unknown, $\mathbf{\Phi}$, we integrate by parts the diffusion term and obtain

$$\int_\Omega \psi \, \frac{\partial \mathbf{\Phi}}{\partial t} \, d\Omega + \int_\Omega \psi \, \mathbf{A}^i(\mathbf{\Phi}) \, \frac{\partial \mathbf{\Phi}}{\partial x_i} \, d\Omega + \int_\Omega \frac{\partial \psi}{\partial x_i} \, \mathbf{K}^{ir}(\mathbf{\Phi}) \, \frac{\partial \mathbf{\Phi}}{\partial x_r} \, d\Omega - \int_\Gamma \psi \, \mathbf{K}^{ir}(\mathbf{\Phi}) \, \frac{\partial \mathbf{\Phi}}{\partial x_r} \, n_i \, d\Gamma = 0 \, , \tag{10}$$

for all $\psi \in W$. The resulting boundary term is used to impose Neumann-like conditions on the fluxes, being $\Gamma = \partial\Omega$ the domain boundary and $n_r$ its exterior unit normal vector. In this paper we consider a zero Neumann boundary condition, i.e. $\int_\Gamma \psi \, \mathbf{K}^{ir}(\mathbf{\Phi}) \, \frac{\partial \mathbf{\Phi}}{\partial x_r} \, n_i \, d\Gamma = 0$ in (10). The problem consists in finding $\mathbf{\Phi} \in L^2(0, T; \, W)^{d+2}$ satisfying (10) for all $\psi \in W$.

### *3.2. Finite element discretization*

We consider $\Omega^h$ a polyhedral approximation of $\Omega$ and we chose a mesh on $\Omega^h$. Formally, a mesh is a partition $\mathcal{P}^h = \{K^m\}_{m=1,\ldots,N_{el}}$ in $N_{el}$ elements, $K^m \subset \Omega^h$, of characteristic length $h^m$, where

$h^m$ is here defined as the shortest edge length of the element. Let $\{\mathbf{x}^p\}_{p=1,\dots,N}$ be the $N$ nodes of the mesh and $\psi_p^h$ the Lagrange polynomial corresponding to node $\mathbf{x}^p$, for $p = 1, \dots, N$. In this work, $\psi_p^h$ are first order polynomials when using triangular elements and bilinear polynomials when using quadrilaterals. From the variational problem (10), a finite element discretization is set up by choosing a suitable test function space, $W^h \subset W$, of finite dimension. Let $W^h$ be the function space generated by $\{\psi_p^h\}_{p=1,\dots,N}$, then the finite element form of the Navier-Stokes equations (7) is written as

$$\int_{\Omega^h} \psi^h \, \frac{\partial \mathbf{\Phi}^h}{\partial t} \, d\Omega^h + \int_{\Omega^h} \psi^h \, \mathbf{A}^i(\mathbf{\Phi}^h) \, \frac{\partial \mathbf{\Phi}^h}{\partial x_i} \, d\Omega^h + \int_{\Omega^h} \frac{\partial \psi^h}{\partial x_i} \, \mathbf{K}^{ir}(\mathbf{\Phi}^h) \, \frac{\partial \mathbf{\Phi}^h}{\partial x_r} \, d\Omega^h \, = 0 \, , \quad (11)$$

for all $\psi^h \in W^h$. The function $\mathbf{\Phi}^h$ is the projection of $\mathbf{\Phi}$ onto $W^h$ and it can be expressed as

$$\mathbf{\Phi}^h(\xi, t) = \sum_{p=1}^{N} \psi_p^h(\xi) \, \mathbf{\Phi}_p^h(t) \, , \quad (12)$$

where $\xi \in \Omega^h$ and $\mathbf{\Phi}_p^h(t)$ is the value of $\mathbf{\Phi}^h$ at node $\mathbf{x}^p$ and time $t$.

### *3.3. Variational multiscale stabilization*

The VMS method is based on the idea that the unknown is the sum of two components, the large scale component and a subscale component. Following this idea, let the test function space, $W$, decompose into the finite element space $W^h$ and a subscale space $\tilde{W}$. That is $W = W^h \oplus \tilde{W}$, where $W^h$ corresponds to the large scales and $\tilde{W}$ is the space that completes $W^h$ inside the test function space $W$. This translates into the decompositions $\mathbf{\Phi} = \mathbf{\Phi}_h + \tilde{\mathbf{\Phi}}$ and $\psi = \psi^h + \tilde{\psi}$ that we plug into the variational form (10) and obtain

$$\begin{aligned} \int_{\Omega^h} (\psi^h + \tilde{\psi}) \, \frac{\partial (\mathbf{\Phi}^h + \tilde{\mathbf{\Phi}})}{\partial t} \, d\Omega^h + \int_{\Omega^h} (\psi^h + \tilde{\psi}) \, \mathbf{A}^i(\mathbf{\Phi}) \, \frac{\partial (\mathbf{\Phi}^h + \tilde{\mathbf{\Phi}})}{\partial x_i} \, d\Omega^h \\ + \int_{\Omega^h} \frac{\partial (\psi^h + \tilde{\psi})}{\partial x_i} \, \mathbf{K}^{ir}(\mathbf{\Phi}) \, \frac{\partial (\mathbf{\Phi}^h + \tilde{\mathbf{\Phi}})}{\partial x_r} \, d\Omega^h \, = 0 \, , \quad (13) \end{aligned}$$

for all $\psi = \psi_h + \tilde{\psi} \in W$. As $W$ is generated by the sum of $W^h$ and $\tilde{W}$, equation (13) splits in two equations as follows

$$\begin{aligned} \int_{\Omega^h} \psi^h \, \frac{\partial \mathbf{\Phi}^h}{\partial t} \, d\Omega^h + \int_{\Omega^h} \psi^h \, \mathbf{A}^i(\mathbf{\Phi}) \, \frac{\partial \mathbf{\Phi}^h}{\partial x_i} \, d\Omega^h + \int_{\Omega^h} \frac{\partial \psi^h}{\partial x_i} \, \mathbf{K}^{ir}(\mathbf{\Phi}) \, \frac{\partial \mathbf{\Phi}^h}{\partial x_r} \, d\Omega^h \\ + \sum_{K \in \mathcal{P}_h} \left( \int_K \psi^h \frac{\partial \tilde{\mathbf{\Phi}}}{\partial t} \, dK + \int_K \psi^h \mathcal{L}(\mathbf{\Phi}) \tilde{\mathbf{\Phi}} \, dK \right) \, = 0 \, , \qquad \forall \psi^h \in W^h \quad (14a) \end{aligned}$$

$$\sum_{K\in\mathcal{P}_h}\int_K \tilde{\psi}\left(\frac{\partial}{\partial t}+\mathcal{L}(\mathbf{\Phi})\right)\tilde{\mathbf{\Phi}}\;dK = -\sum_{K\in\mathcal{P}_h}\int_K \tilde{\psi}\left(\frac{\partial}{\partial t}+\mathcal{L}(\mathbf{\Phi})\right)\mathbf{\Phi}^h\;dK\;, \qquad \forall\tilde{\psi}\in\tilde{W} \quad (14b)$$

where

$$\mathcal{L}(\mathbf{\Phi}) = \mathbf{A}^i(\mathbf{\Phi})\frac{\partial}{\partial x_i} - \frac{\partial}{\partial x_i}\left(\mathbf{K}^{ir}(\mathbf{\Phi})\frac{\partial}{\partial x_r}\right)\;, \tag{15}$$

is the original space differential operator. We replaced $\int_{\Omega^h}$ by $\sum_{K\in\mathcal{P}_h}\int_K$ in the subscale terms of (14) because the subscales are defined inside the elements but not necessarily on their boundaries. As it is done in [10, 14], we chose $\tilde{W}$ orthogonal to $W^h$.

The large scale equation (14a) is solved numerically to compute an approximate solution, $\mathbf{\Phi}^h$, to our problem. The subscale equation (14b) is used to model the subscales, that is to find an expression for $\tilde{\mathbf{\Phi}}$ which will be plugged into the large scale equation. In what follows, we enumerate some simplifications done on the large scale and the subscale equations.

Concerning the large scale equation (14a), we make the following assumptions that are tested in the literature:

1. Because we took $\tilde{W}$ orthogonal to $W^h$, then we have

$$\int_K \psi^h\frac{\partial\tilde{\mathbf{\Phi}}}{\partial t}\;dK = 0\;. \tag{16}$$

2. To avoid the space derivatives of the subscale, we integrate by parts the last term of (14a) and we suppose the arising boundary terms to be zero, that is

$$\int_K \psi^h\;\mathcal{L}(\mathbf{\Phi})\tilde{\mathbf{\Phi}}\;dK = \int_K \mathcal{L}^*(\mathbf{\Phi})\psi^h\;\tilde{\mathbf{\Phi}}\;dK\;, \tag{17}$$

where the dual operator is

$$\begin{aligned}\mathcal{L}^*(\mathbf{\Phi})\psi^h &= -\frac{\partial}{\partial x_i}\left(\psi^h\;\mathbf{A}^i(\mathbf{\Phi})\right) - \frac{\partial}{\partial x_r}\left(\frac{\partial\psi^h}{\partial x_i}\;\mathbf{K}^{ir}(\mathbf{\Phi})\right)\\ &= -\frac{\partial\psi^h}{\partial x_i}\;\mathbf{A}^i(\mathbf{\Phi}) - \psi^h\;\frac{\partial\mathbf{A}^i(\mathbf{\Phi})}{\partial x_i} - \frac{\partial^2\psi^h}{\partial x_r\partial x_i}\;\mathbf{K}^{ir}(\mathbf{\Phi}) - \frac{\partial\psi^h}{\partial x_i}\;\frac{\partial\mathbf{K}^{ir}(\mathbf{\Phi})}{\partial x_r}\;.\end{aligned} \tag{18}$$

3. For the sake of algorithmic simplicity, we make the approximations $\mathbf{A}^i(\mathbf{\Phi}) \approx \mathbf{A}^i(\mathbf{\Phi}^h)$ and $\mathbf{K}^{ir}(\mathbf{\Phi}) \approx \mathbf{K}^{ir}(\mathbf{\Phi}^h)$ (see, for example, [18]). For incompressible flow, they preserve the exact form in [14]; this requires the storage of the subscale at each iteration.

We observe that imposing equation (14a) to hold for all $\psi^h \in W^h$ is equivalent to imposing it to hold for all $\psi^h_p$, $p\in\{1,\ldots,N\}$, because the test functions space $W^h$ is generated by $\{\psi^h_p\}_{p=1,\ldots,N}$.

This observation together with the last assumptions lead to the reformulation of (14a) as

$$\int_{\Omega^h} \psi_p^h \, \frac{\partial \mathbf{\Phi}^h}{\partial t} \, d\Omega^h + \int_{\Omega^h} \psi_p^h \, \mathbf{A}^i(\mathbf{\Phi}^h) \, \frac{\partial \mathbf{\Phi}^h}{\partial x_i} \, d\Omega^h + \int_{\Omega^h} \frac{\partial \psi_p^h}{\partial x_i} \, \mathbf{K}^{ir}(\mathbf{\Phi}^h) \, \frac{\partial \mathbf{\Phi}^h}{\partial x_r} \, d\Omega^h + \sum_{K \in \mathcal{P}_h} \int_K \mathcal{L}^*(\mathbf{\Phi}^h) \psi_p^h \, \tilde{\mathbf{\Phi}} \, dK \, = 0 \, , \quad (19)$$

holding for all $p \in \{1, \ldots, N\}$. The stabilization term is the last term in equation (19). This term represents the effect of the subscales on the large scales.

Concerning the subscale equation (14b), we make the approximation $\mathcal{L}(\mathbf{\Phi}) \approx \mathcal{L}(\mathbf{\Phi}^h)$ (same as in the third point above). Thus (14b) becomes

$$\sum_{K \in \mathcal{P}_h} \int_K \tilde{\psi} \left( \frac{\partial}{\partial t} + \mathcal{L}(\mathbf{\Phi}^h) \right) \tilde{\mathbf{\Phi}} \, dK = - \sum_{K \in \mathcal{P}_h} \int_K \tilde{\psi} \, \left( \frac{\partial}{\partial t} + \mathcal{L}(\mathbf{\Phi}^h) \right) \mathbf{\Phi}^h \, dK \, , \quad (20)$$

for all $\tilde{\psi} \in \tilde{W}$. Equation (20) will be the departing point of any model for the VMS subscales.

### *3.4. Modeling the VMS subscales*

Here we present two options for the modeling of the subscale, which is a topic of active research still today [32]. The first option, in Section 3.4.1, assumes the subscale to have the classical structure, that is, the product of a parameter $\tau$ times the residual of the problem. The parameter $\tau$ that we use is a straight adaptation of the one used in [14] in the context of the incompressible flow equations. The second option, in Section 3.4.2, inspired by what is done in [10], uses the Fourier transform to model the subscale, without assuming the classical structure.

#### *3.4.1. Diagonal $\tau$ subscale*

We take the subscale equation (20) and we consider the hypotheses of quasi-static subscales (refer to [10]), which means that $\frac{\partial \tilde{\mathbf{\Phi}}}{\partial t} \approx 0$. This way we avoid the time tracking of the subscales. For a description of how the subscales can be tracked when solving the incompressible equations, refer to [14]. On the other hand, because we took $\tilde{W}$ orthogonal to $W^h$, we have $\int_K \tilde{\psi} \, \frac{\partial \mathbf{\Phi^h}}{\partial t} \, dK = 0$. Thus equation (20) becomes

$$\sum_{K \in \mathcal{P}_h} \int_K \tilde{\psi} \, \mathcal{L}(\mathbf{\Phi}^h) \, \tilde{\mathbf{\Phi}} \, dK = - \sum_{K \in \mathcal{P}_h} \int_K \tilde{\psi} \, \mathcal{L}(\mathbf{\Phi}^h) \, \mathbf{\Phi}^h \, dK \, , \quad (21)$$

for all $\tilde{\psi} \in \tilde{W}$. From (21) we obtain for every $K \in \mathcal{P}_h$,

$$\mathcal{L}(\mathbf{\Phi}^h) \, \tilde{\mathbf{\Phi}} \, = \, \mathbf{r}(\mathbf{\Phi}^h) + \mathbf{\Psi}^h_{\text{ort}} \, , \quad (22)$$

where

$$\mathbf{r}(\mathbf{\Phi}^h) \,=\, -\,\mathcal{L}(\mathbf{\Phi}^h)\mathbf{\Phi}^h \,, \tag{23}$$

is the space residual of the large scales equation and $\mathbf{\Psi}^h_{\rm ort}$ is the projection of $\mathcal{L}(\mathbf{\Phi}^h)\,\tilde{\mathbf{\Phi}} - \mathbf{r}(\mathbf{\Phi}^h)$ in $W^h$ (see [14, 10]). In this work we consider $\mathbf{\Psi}^h_{\rm ort}$ to be zero. If we call $\tau$ an approximation of $(\mathcal{L}(\mathbf{\Phi}^h))^{-1}$, from (22), the compressible flow subscales $\tilde{\mathbf{\Phi}}$ can be approximated in every element $K \in \mathcal{P}^h$ as

$$\tilde{\mathbf{\Phi}} = \tau\ \mathbf{r}(\mathbf{\Phi}^h)\ . \tag{24}$$

From (24) we see the local nature of the subscales that are meant to exist only where the residuals are high. Most of the models describe the subscale in the form of equation (24), i.e. as the product of a parameter $\tau$ times the residual of the equation. There exist, for compressible flow, many proposals for the definition of $\tau$ in the literature, some of them are found in [2, 4], in the context of SUPG; in [6], in the context of GLS; and in [18], in the context of VMS. Following the line set for incompressible flow in [14], parameter $\tau$, is here defined as

$$\tau = \left( \frac{\|\mathbf{u}\| + c}{h} + \frac{4\,\mu}{\rho\, h^2} \right)^{-1} \ . \tag{25}$$

Now, expression (24) using (25) is plugged into equation (19) to find an approximate solution of problem (7). Looking at (25), we note that $\tau$ depends on the speed of the sound, which is not the case of the incompressible flow formulation of [14]. However it is the case of other compressible flow formulations, for instance, in [2, 4, 18]. In fact, $\|\mathbf{u}\| + c$ is the maximum characteristic propagation speed of the compressible Navier-Stokes equations [33, 23].

*3.4.2. Fourier subscale*

Here we propose a different method, which takes as a starting point the Fourier approach of [10]. For every $K \in \mathcal{P}_h$ the time discretized subscale equation (20) can be written as

$$\sum_{K\in\mathcal{P}_h} \int_K \tilde{\psi} \left( \frac{\tilde{\mathbf{\Phi}}^{n+1} - \tilde{\mathbf{\Phi}}^{n}}{\Delta t} + \mathcal{L}(\mathbf{\Phi}^{h,n})\,\tilde{\mathbf{\Phi}}^{n+1} \right)\, dK \,= \\ - \sum_{K\in\mathcal{P}_h} \int_K \tilde{\psi} \left( \frac{\mathbf{\Phi}^{h,n+1} - \mathbf{\Phi}^{h,n}}{\Delta t} + \mathcal{L}(\mathbf{\Phi}^{h,n})\,\mathbf{\Phi}^{h,n} \right)\, dK \ , \tag{26}$$

where superscripts $n$ and $n+1$ account for the last and the current time steps, respectively. We move $\frac{-\tilde{\mathbf{\Phi}}^n}{\Delta t}$ from the left to the right side in (26) and obtain

$$\sum_{K\in\mathcal{P}_h}\int_K \tilde{\psi}\left(\frac{1}{\Delta t}+\mathcal{L}(\mathbf{\Phi}^{h,n})\right)\tilde{\mathbf{\Phi}}^{n+1}\,dK = -\sum_{K\in\mathcal{P}_h}\int_K \tilde{\psi}\left(\frac{\mathbf{\Phi}^{h,n+1}-\mathbf{\Phi}^n}{\Delta t}+\mathcal{L}(\mathbf{\Phi}^{h,n})\,\mathbf{\Phi}^{h,n}\right)\,dK\ . \quad (27)$$

We approximate $\frac{\mathbf{\Phi}^{h,n+1}-\mathbf{\Phi}^n}{\Delta t}$ by $\frac{\mathbf{\Phi}^{h,n+1}-\mathbf{\Phi}^{h,n}}{\Delta t}$ in (27). On the other hand, because we took $\tilde{W}$ orthogonal to $W^h$, we have $\int_K \tilde{\psi}\,\frac{\mathbf{\Phi}^{h,n+1}-\mathbf{\Phi}^{h,n}}{\Delta t}\,dK = 0$. Then (27) becomes

$$\sum_{K\in\mathcal{P}_h}\int_K \tilde{\psi}\left(\frac{1}{\Delta t}+\mathcal{L}(\mathbf{\Phi}^{h,n})\right)\tilde{\mathbf{\Phi}}^{n+1}\,dK = -\sum_{K\in\mathcal{P}_h}\int_K \tilde{\psi}\,\mathcal{L}(\mathbf{\Phi}^{h,n})\,\mathbf{\Phi}^{h,n}\,dK\ . \quad (28)$$

Now we proceed as we did for equation (22). From the subscale equation (28), we obtain for every $K\in\mathcal{P}_h$

$$\left(\frac{1}{\Delta t}+\mathcal{L}(\mathbf{\Phi}^{h,n})(\mathbf{x})\right)\tilde{\mathbf{\Phi}}^{n+1}(\mathbf{x}) = \mathbf{r}(\mathbf{\Phi}^{h,n})(\mathbf{x})+\mathbf{\Psi}^h_{\text{ort}}(\mathbf{x})\ , \quad (29)$$

where the space residual $\mathbf{r}$ is defined in (23) and $\mathbf{\Psi}^h_{\text{ort}}$ is the projection of $\left(\frac{1}{\Delta t}+\mathcal{L}(\mathbf{\Phi}^{h,n})\right)\tilde{\mathbf{\Phi}}^{n+1} - \mathbf{r}(\mathbf{\Phi}^{h,n})$ in $W^h$. As a first approximation we consider $\mathbf{\Psi}^h_{\text{ort}}$ to be zero in this paper. Now we want to transform equation (29) into the Fourier space. Given an integrable function $f$ defined on each element K, its Fourier transform writes

$$\widehat{f}(\omega) = \int_K f(\mathbf{x})e^{-\mathbf{i}\,\theta_k\omega_k x_k}\,d\mathbf{x}\ , \quad (30)$$

where $k=1,\dots,d$, $\mathbf{i}$ is the imaginary unit, $\omega\in\mathbb{R}^d$ is the Fourier parameter, $\theta_k=\frac{2\pi}{h_k}$ , and $h_k$ is the characteristic length for each space component. Its inverse transform writes

$$f(\mathbf{x}) = \int_{\mathbb{R}^d}\widehat{f}(\omega)e^{\mathbf{i}\,\theta_k\omega_k x_k}\,d\omega\ . \quad (31)$$

The Fourier transform of its first and second degree partial derivatives write

$$\widehat{\frac{\partial f}{\partial x_i}}(\omega) = \mathbf{i}\,\theta_i\omega_i\,\widehat{f}(\omega)+\int_\Gamma n_i\,e^{-\mathbf{i}\,\theta_k\omega_k x_k}f(\mathbf{x})\,d\mathbf{x}\ , \quad (32)$$

$$\begin{aligned}\widehat{\frac{\partial^2 f}{\partial x_i\partial x_r}}(\omega) =& -\theta_i\theta_r\omega_i\omega_r\,\widehat{f}(\omega)+\int_\Gamma n_i\,e^{-\mathbf{i}\,\theta_k\omega_k x_k}\frac{\partial f}{\partial x_r}(\mathbf{x})\,d\mathbf{x}\\ &+\int_\Gamma n_r\,\mathbf{i}\,\theta_i\omega_i\,e^{-\mathbf{i}\,\theta_k\omega_k x_k}f(\mathbf{x})\,d\mathbf{x}\ ,\end{aligned} \quad (33)$$

respectively, where $k, i = 1, \ldots, d$, $\mathbf{n}$ is the exterior normal to $K$. As it is done in [10], we assume that

$$\widehat{\frac{\partial \tilde{\mathbf{\Phi}}}{\partial x_i}} \approx \mathbf{i}\, \theta_i \omega_i\, \hat{\tilde{\mathbf{\Phi}}} \,, \tag{34}$$

$$\widehat{\frac{\partial^2 \tilde{\mathbf{\Phi}}}{\partial x_i \partial x_r}} \approx -\theta_i \theta_r \omega_i \omega_r\, \hat{\tilde{\mathbf{\Phi}}} \,. \tag{35}$$

Thus the Fourier transform of the equation (29) writes

$$\left(\frac{1}{\Delta t} + L(\omega)\right) \hat{\tilde{\mathbf{\Phi}}}^{n+1}(\omega) = \widehat{\mathbf{r}(\mathbf{\Phi}^{h,n})}(\omega) \,, \tag{36}$$

where we approximate the Fourier's transform of $\mathcal{L}$ as

$$L(\omega) = \mathbf{i}\, \theta_i \omega_i\, \bar{\mathbf{A}}^i(\mathbf{\Phi}^{h,n}) + \theta_i \theta_r \omega_i \omega_r\, \bar{\mathbf{K}}^{ir}(\mathbf{\Phi}^{h,n}) \,. \tag{37}$$

Bars over $\mathbf{A}^i$ and $\mathbf{K}^{ir}$ notes their mean value on $K$. We observe from (37) that the partial derivatives in $\mathcal{L}$ disappear when transforming it to the Fourier space. From (36) we obtain an expression for the subscale transform

$$\hat{\tilde{\mathbf{\Phi}}}^{n+1}(\omega) = \mathcal{T}(\omega)\, \widehat{\mathbf{r}(\mathbf{\Phi}^{h,n})}(\omega) \tag{38}$$

where $\mathcal{T}(\omega) = \left(\frac{1}{\Delta t} + L(\omega)\right)^{-1}$. Finally, to model the subscales, we transform back to the physical space, obtaining for all $\mathbf{y} \in K$

$$\tilde{\mathbf{\Phi}}^{n+1}(\mathbf{y}) = \int_{\mathbb{R}^d} \int_K \tau(\omega, \mathbf{x}, \mathbf{y})\, \mathbf{r}(\mathbf{\Phi}^{h,n})(\mathbf{x})\, d\mathbf{x}\, d\omega \,, \tag{39}$$

where

$$\tau(\omega, \mathbf{x}, \mathbf{y}) = Re\left(\mathcal{T}(\omega)\right)\, \cos(\theta_k \omega_k\, (x_k - y_k)) + Im\left(\mathcal{T}(\omega)\right)\, \sin(\theta_k \omega_k\, (x_k - y_k)) \,. \tag{40}$$

Lets discretize the integral $\int_{\mathbb{R}^d} (\cdot)\, d\omega$ and approximate it as the finite sum $\sum_{\omega \in D} (\cdot)$. Observe that $L(-\omega) = \overline{L(\omega)}$, then $\mathcal{T}(-\omega) = \overline{\mathcal{T}(\omega)}$ and $\tau(-\omega, \mathbf{x}, \mathbf{y})) = \tau(\omega, \mathbf{x}, \mathbf{y})$. As a consequence, only half of the Fourier domain $\mathbb{R}^d$ needs to be considered, and we can define $D = D_1 \cap D_2 \subset \mathbb{Z}^d$, where

$$D_1 = \{0\} \cup \{\omega_1 > 0\} \cup \{\omega_2 > 0,\, \omega_1 = 0\} \cup \cdots \cup \{\omega_d > 0,\, \omega_k = 0, \quad \forall k = 1, \ldots, d-1\} \subset \mathbb{Z}^d \,, \tag{41}$$

$$D_2 = \{|\omega_k| \leq M_{\text{freq}} \quad \forall k = 1, \ldots, d\} \,. \tag{42}$$

In the definition of $D_2$, $M_{\text{freq}} \in \mathbb{Z}$, $M_{\text{freq}} \geq 0$, limits the extension of the set $D$ to a finite number of Fourier frequencies. In the applications, $M_{\text{freq}}$ typically takes the value of 0, 1, 2, or 3. Finally we obtain

$$\tilde{\mathbf{\Phi}}^{n+1}(\mathbf{y}) = \int_K \Delta t\ \mathbf{r}(\mathbf{\Phi}^{h,n})(\mathbf{x})\ d\mathbf{x}\ +\ 2 \sum_{\omega \in D \setminus \{0\}} \int_K \tau(\omega, \mathbf{x}, \mathbf{y})\ \mathbf{r}(\mathbf{\Phi}^{h,n})(\mathbf{x})\ d\mathbf{x}\ . \tag{43}$$

Now, expression (43) is plugged into equation (19) to find an approximate solution of problem (7). Observe that when we take $M_{\text{freq}} = 0$, we get, for all $y \in K$,

$$\tilde{\mathbf{\Phi}}^{n+1}(\mathbf{y}) = \int_K \Delta t\ \mathbf{r}(\mathbf{\Phi}^{h,n})(\mathbf{x})\ d\mathbf{x}\ . \tag{44}$$

The time step $\Delta t$ in (43) and (44) is the one that we will define in equation (49). The above computations for the Fourier subscale are done for structured meshes but used for structured and unstructured ones.

### *3.5. Time discretization*

The time discretization of (19) is here done by an explicit scheme, giving

$$\begin{aligned}\int_{\Omega^h} \psi_p^h\ \frac{\mathbf{\Phi}^{h,n+1} - \mathbf{\Phi}^{h,n}}{\Delta t}\ d\Omega^h + \int_{\Omega^h} \psi_p^h\ \mathbf{A}^i(\mathbf{\Phi}^{h,n})\ \frac{\partial \mathbf{\Phi}^{h,n}}{\partial x_i}\ d\Omega^h \\ + \int_{\Omega^h} \frac{\partial \psi_p^h}{\partial x_i}\ \mathbf{K}^{ir}(\mathbf{\Phi}^{h,n})\ \frac{\partial \mathbf{\Phi}^{h,n}}{\partial x_r}\ d\Omega^h + \sum_{K \in \mathcal{P}_h} \int_K \mathcal{L}(\mathbf{\Phi}^{h,n})^* \psi_p^h\ \tilde{\mathbf{\Phi}}^{n+1}\ dK\ = 0\ ,\end{aligned} \tag{45}$$

holding for all $p \in \{1, \ldots, N\}$. The superscripts $n+1$ and $n$ indicate the value at the current and the previous time step, respectively. The value of $\tilde{\mathbf{\Phi}}^{n+1}$ is computed from the information of the previous time step $n$. When the diagonal $\tau$ subscale is used (24), the subscale at time step $n+1$ reads

$$\tilde{\mathbf{\Phi}}^{n+1} = \tau^n\ \mathbf{r}(\mathbf{\Phi}^{h,n})\ , \tag{46}$$

where the residual (23) at time $n$ reads

$$\mathbf{r}(\mathbf{\Phi}^{h,n})\ =\ -\mathcal{L}(\mathbf{\Phi}^{h,n})\mathbf{\Phi}^{h,n} = -\mathbf{A}^i(\mathbf{\Phi}^{h,n})\frac{\partial \mathbf{\Phi}^{h,n}}{\partial x_i} + \frac{\partial}{\partial x_i}\left(\mathbf{K}^{ir}(\mathbf{\Phi}^{h,n})\frac{\partial \mathbf{\Phi}^{h,n}}{\partial x_r}\right)\ , \tag{47}$$

and $\tau^n$ is the value of $\tau$, explicitly defined in (25), at time $n$. When the Fourier subscale is used, then $\tilde{\mathbf{\Phi}}^{n+1}$ is defined from (43).

From the CFL condition [34] a time step inside each element is defined as

$$\Delta t^{\,el} = C\,\left(\frac{\|\mathbf{u}\| + c}{h} + \frac{4\,\mu}{\rho\,h^2}\right)^{-1}\,, \tag{48}$$

where $C \in (0,1)$ is the CFL number and $h$ is the smallest edge length of the element. The elemental time step (48) is interpolated on the nodes of the grid, obtaining a local time step $\Delta t^{\,p}$ at each node $\mathbf{x}^p$ of the grid, for $p = 1, \ldots, N$. The global time step here used is computed as the minimum time step of the domain:

$$\Delta t = \min_{p=1,\ldots,N}\{\Delta t^{\,p}\}\,. \tag{49}$$

Inserting equality (12) in (45), a linear system of $N(d+2)$ equations is obtained:

$$\mathbf{M}\,\frac{\mathbf{\Phi}^{h,n+1} - \mathbf{\Phi}^{h,n}}{\Delta t} = \mathbf{G}(\mathbf{\Phi}^{h,n}) + \mathbf{S}(\mathbf{\Phi}^{h,n}, \tilde{\mathbf{\Phi}}^{n+1})\,, \tag{50}$$

where

1. $\mathbf{\Phi}^h$ is here the nodal vector of unknowns of dimension $N(d+2)$. It is made by assembly of the vectors $\mathbf{\Phi}^h_p$, for $p = 1, \ldots, N$.
2. $\mathbf{M}$ is the global Mass matrix, it has dimension $N(d+2) \times N(d+2)$. It is a block matrix composed of $N^2$ blocks $\mathbf{M}^{pq}$ of dimension $(d+2) \times (d+2)$,

$$\mathbf{M}^{pq} = \int_{\Omega^h} \psi^h_p \psi^h_q \, d\Omega^h \, \mathbf{I}_{d+2}\,, \tag{51}$$

   where $p, q = 1, \ldots, N$ and $\mathbf{I}_{d+2}$ is the identity matrix of dimension $(d+2) \times (d+2)$.
3. $\mathbf{G}$ and $\mathbf{S}$ are the Galerkin and stabilization vector terms, respectively. They are constructed by assembly of the following $N$ local vectors of dimension $d+2$:

$$\mathbf{G}^p = -\left(\int_{\Omega^h} \psi^h_p \; \mathbf{A}^i(\mathbf{\Phi}^{h,n})\,\frac{\partial \mathbf{\Phi}^{h,n}}{\partial x_i}\, d\Omega^h + \int_{\Omega^h} \frac{\partial \psi^h_p}{\partial x_i}\,\mathbf{K}^{ir}(\mathbf{\Phi}^{h,n})\,\frac{\partial \mathbf{\Phi}^{h,n}}{\partial x_r}\, d\Omega^h\right)\,, \tag{52}$$

$$\mathbf{S}^p = -\sum_{K \in \mathcal{P}_h} \int_K \mathcal{L}(\mathbf{\Phi}^{h,n})^* \psi^h_p \; \tilde{\mathbf{\Phi}}^{n+1}\, dK\,, \tag{53}$$

   respectively, for $p = 1, \ldots, N$.

All the integrals above are approximated by the Gaussian quadrature rule that, for a function $f$, writes

$$\int_{K^m} f(\mathbf{x})\, dK^m = \int_I f(\mathcal{H}^m(\xi))\,|J^m(\xi)|\, d\xi \approx \sum_{p=1}^{N_{Gauss}} f(\mathcal{H}^m(\xi^p))\,|J^m(\xi^p)|\,\omega^p, \tag{54}$$

where $I = [-1,1] \times [-1,1]$ is a reference element, $\mathcal{H}^m$ a bijection from $I$ to the element $K^m$, $J^m = \frac{\mathrm{d}\mathcal{H}^m}{\mathrm{d}\xi}$ the $\mathcal{H}^m$ Jacobian matrix, $|J^m|$ its determinant, $N_{Gauss}$ is the number of integration Gauss points $\xi^p$ inside the element $K^m$, and $\omega^p$ its weight.

$\mathbf{M}$ is diagonalized by lumping techniques [35] in order to avoid its inversion when open integration rules are used. From equation (50), the value of $\mathbf{\Phi}^{h,n+1}$ at each node of the computational grid is obtained as

$$\mathbf{\Phi}^{h,n+1} = \mathbf{\Phi}^{h,n} + \Delta t\, \mathbf{M}^{-1} \left( \mathbf{G}(\mathbf{\Phi}^{h,n}) + \mathbf{S}(\mathbf{\Phi}^{h,n}, \tilde{\mathbf{\Phi}}^{n+1}) \right) . \tag{55}$$

VMS stabilization term (53) with the diagonal $\tau$ subscale (46), can be compared with the corresponding compressible SUPG ([2, 3, 4, 5]), GLS ([6]), and Rispoli's VMS ([18]) stabilization terms. When the diagonal $\tau$ subscale (46) is used, our VMS stabilization term (53) reads

$$\mathbf{S}^p = - \sum_{K \in \mathcal{P}_h} \int_K \left( -\frac{\partial \psi_p^h}{\partial x_i}\, \mathbf{A}^i(\mathbf{\Phi}^{h,n}) - \psi_p^h\, \frac{\partial \mathbf{A}^i(\mathbf{\Phi}^{h,n})}{\partial x_i} \right.$$
$$\left. - \frac{\partial^2 \psi_p^h}{\partial x_r \partial x_i}\, \mathbf{K}^{ir}(\mathbf{\Phi}^{h,n}) - \frac{\partial \psi_p^h}{\partial x_i}\, \frac{\partial \mathbf{K}^{ir}(\mathbf{\Phi}^{h,n})}{\partial x_r} \right) \tau^n\, \mathbf{r}(\mathbf{\Phi}^{h,n})\, dK . \tag{56}$$

The corresponding SUPG stabilization term reads

$$\mathbf{S}^p_{\mathrm{SUPG}} = - \sum_{K \in \mathcal{P}_h} \int_K - \frac{\partial \psi_p^h}{\partial x_i}\, \mathbf{A}^i(\mathbf{\Phi}^{h,n})\, \tau^n_{\mathrm{SUPG}}\, \mathbf{r}_t(\mathbf{\Phi}^{h,n})\, dK , \tag{57}$$

the GLS stabilization term reads

$$\mathbf{S}^p_{\mathrm{GLS}} = - \sum_{K \in \mathcal{P}_h} \int_K \left( -\frac{\partial \psi_p^h}{\partial x_i}\, \mathbf{A}^i(\mathbf{\Phi}^{h,n}) \right.$$
$$\left. + \frac{\partial^2 \psi_p^h}{\partial x_i \partial x_r}\, \mathbf{K}^{ir}(\mathbf{\Phi}^{h,n}) + \frac{\partial \psi_p^h}{\partial x_r}\, \frac{\partial \mathbf{K}^{ir}(\mathbf{\Phi}^{h,n})}{\partial x_i} \right) \tau^n_{\mathrm{GLS}}\, \mathbf{r}_t(\mathbf{\Phi}^{h,n})\, dK , \tag{58}$$

and Rispoli's VMS stabilization term (when $\psi^h$ does not depend on the time variable $t$, as it is the case in our work) reads

$$\mathbf{S}^p_{\mathrm{Rispoli}} = - \sum_{K \in \mathcal{P}_h} \int_K \left( -\frac{\partial \psi_p^h}{\partial x_i}\, \mathbf{A}^i(\mathbf{\Phi}^{h,n}) \right.$$
$$\left. - \frac{\partial^2 \psi_p^h}{\partial x_r \partial x_i}\, \mathbf{K}^{ir}(\mathbf{\Phi}^{h,n}) - \frac{\partial \psi_p^h}{\partial x_i}\, \frac{\partial \mathbf{K}^{ir}(\mathbf{\Phi}^{h,n})}{\partial x_r} \right) \tau^n_{\mathrm{Rispoli}}\, \mathbf{r}_t(\mathbf{\Phi}^{h,n})\, dK . \tag{59}$$

The residual $\mathbf{r}(\mathbf{\Phi}^{h,n})$ in (59) is defined by (47). Remark that, as we took orthogonal subscales, the time derivatives $\frac{\partial \mathbf{\Phi}^h}{\partial t}$

to move because of the discontinuous initial condition of the left and right states which entails a shock wave that propagates to both left and right sides. This leads to a maximum Mach number of 0.828 approximately.

Our computational domain is a two-dimensional rectangular tube. This tube is partitioned in the horizontal direction with a mesh of 400 rectangles and 802 nodes, no partition is done in the vertical direction as shown in Fig. 1. The one-dimensionality of the original problem is assured by imposing $u_2 = 0$ boundary condition on the upper and lower walls, that is, in all the nodes. The left and right boundaries are left free of boundary conditions. We use a CFL number of 0.8 in the computation of the time step and 4 integration Gauss points. No shock capturing is used for this case.

In Fig. 2 the exact analytical solution for the density is plotted and compared to the corresponding numerical solution, using the diagonal $\tau$ subscale as well as the Fourier subscale for $M_{\text{freq}} = 0$ and $M_{\text{freq}} = 2$. We see that the shock location is correctly predicted. In some of the cases the solution has small undershoots near the shock, these oscillations are, however, localized and do not corrupt the solution away from the shock. When $M_{\text{freq}} = 2$ is used, the instabilities near the shocks disappear and the solution is more diffusive. In Fig. 3 we show the behavior of the solution when the number of Fourier frequencies and Gauss points are increased. As expected, the solution is smoother when $M_{\text{freq}}$ is increased, and slightly less diffusive when more Gauss points are used.

In order to show the operability of the scheme through a wide range of Mach numbers, the same problem with two different settings on the initial conditions has been solved as well, giving a supersonic case and a very subsonic case. The supersonic shock tube reaches a Mach number of around 10 and is generated using a large discontinuity jump in the initial data: the left density is set to 1 and the right density is set to $10^{-10}$, and the left total energy is set to 2.5 and the right total energy is set to $2.5 \times 10^{-10}$. Comparative results of the supersonic shock tube for the diagonal $\tau$ subscale and the Fourier subscale are displayed in Fig. 4. We observe that the results are very similar for both cases. Concerning the very subsonic tube, it reaches a maximum Mach number of around $1.4 \times 10^{-6}$. The initial conditions are: the left density is set to 1 and the right density is set to 0.99998, and the left energy is set to 2.5 and the right energy is set to 2.49999. The results obtained for this subsonic case using the diagonal $\tau$ subscale and the Fourier subscale are almost identical. In Fig. 5 we show the results using the diagonal $\tau$ subscale. Both shock tube

configurations are solved using a CFL number of 0.8 for the time step, 4 integration Gauss points, and $M_{\text{freq}} = 1$ for the Fourier subscale. No shock capturing is used in any of the configurations for this case.

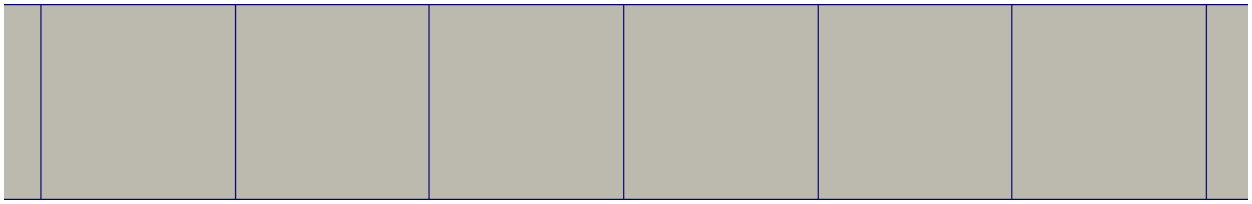

Figure 1: Sod's shock tube. Close-up of the computational mesh.

(a) Diagonal $\tau$ subscale

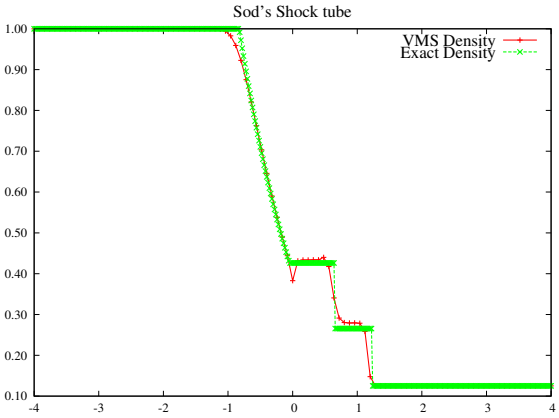


(b) Fourier subscale, $M_{\text{freq}} = 0$

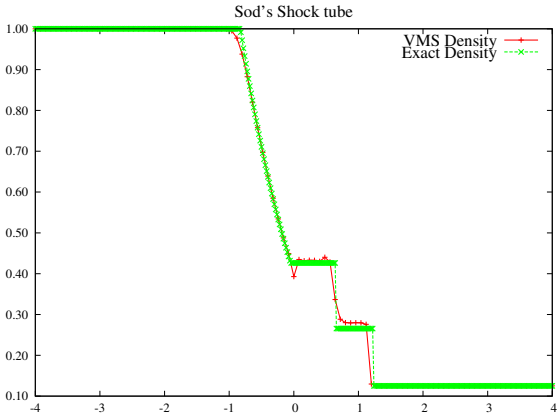


(c) Fourier subscale, $M_{\text{freq}} = 2$

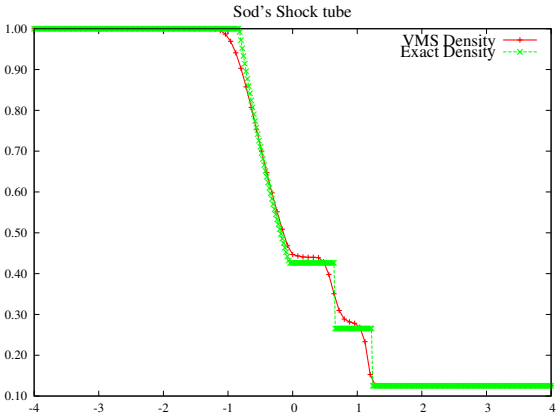


Figure 2: Sod's shock tube. Comparison of the density analytical result (green line) and the corresponding solution of the simulation (red line) using the diagonal $\tau$ subscale and two different configurations of the Fourier subscale. We use 4 integration Gauss points. The solution is advanced to $t = 0.7$.

(a) 4 Gauss points, $M_{\text{freq}} = 0$

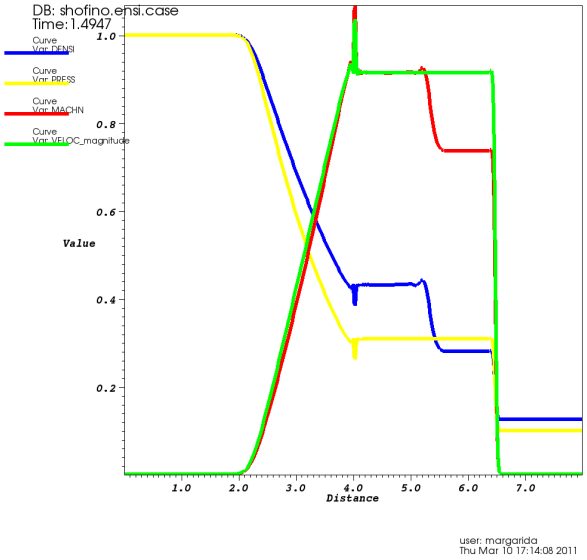


(b) 9 Gauss points, $M_{\text{freq}} = 0$

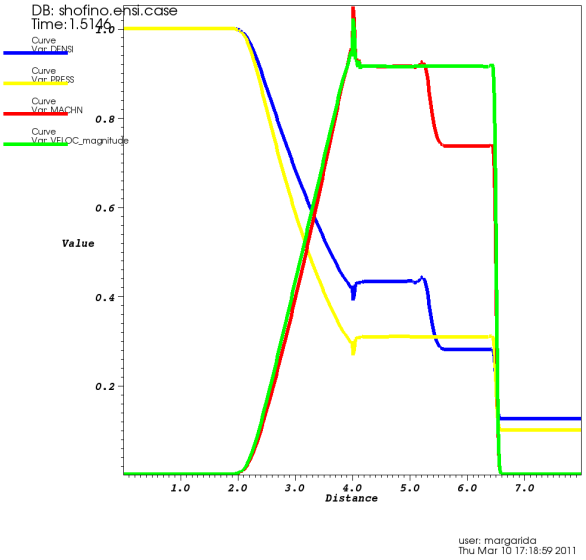


(c) 4 Gauss points, $M_{\text{freq}} = 1$

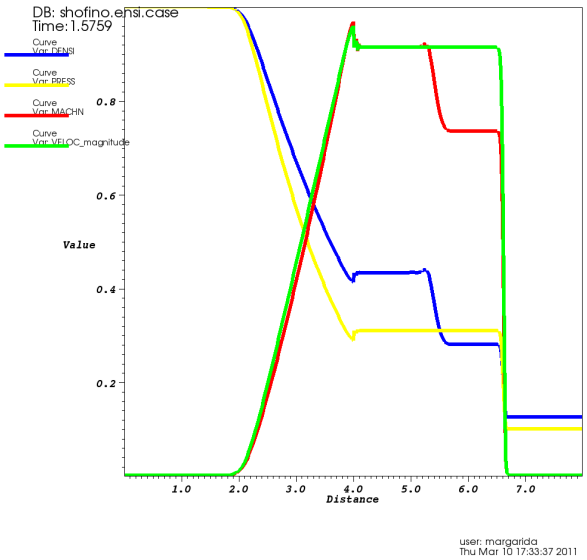


(d) 9 Gauss points, $M_{\text{freq}} = 1$

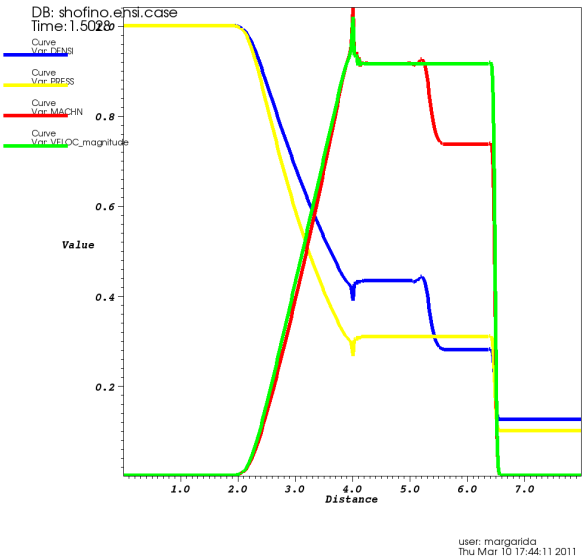

(e) 4 Gauss points, $M_{\text{freq}} = 2$

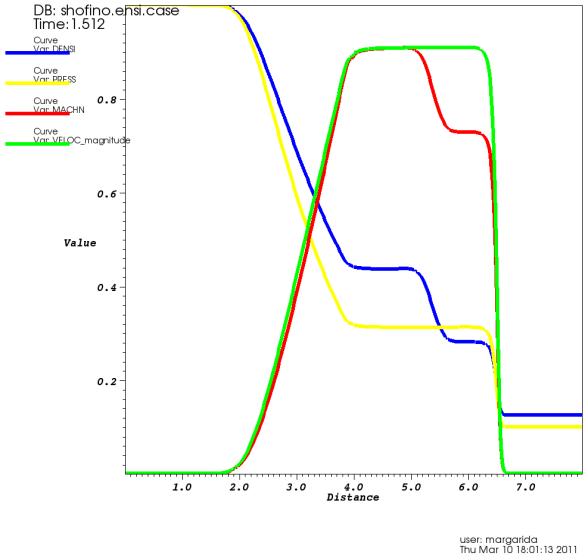


(f) 9 Gauss points, $M_{\text{freq}} = 2$

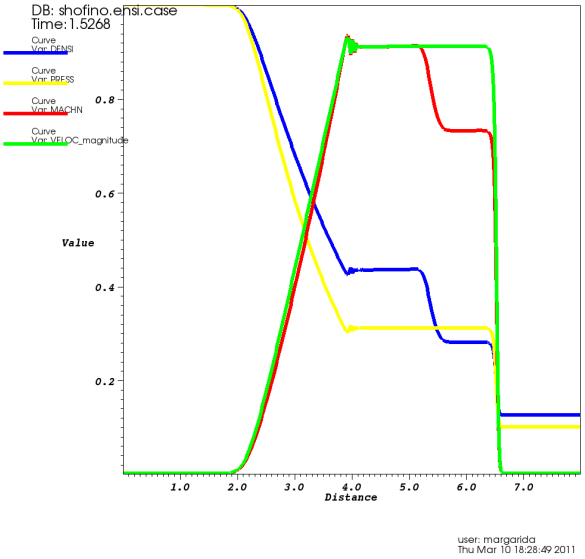


(g) 4 Gauss points, $M_{\text{freq}} = 3$

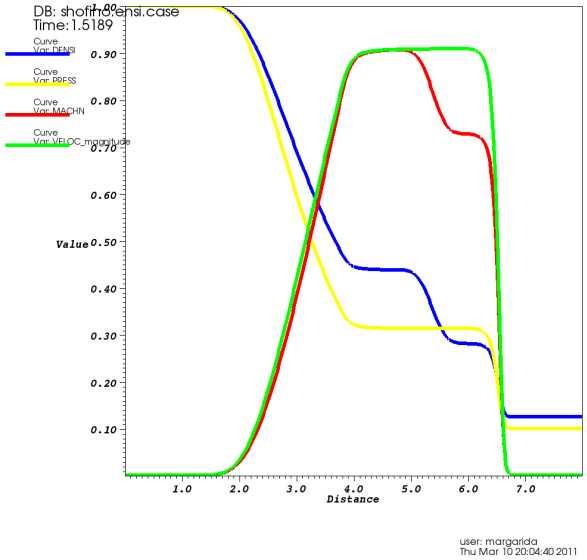


(h) 9 Gauss points, $M_{\text{freq}} = 3$

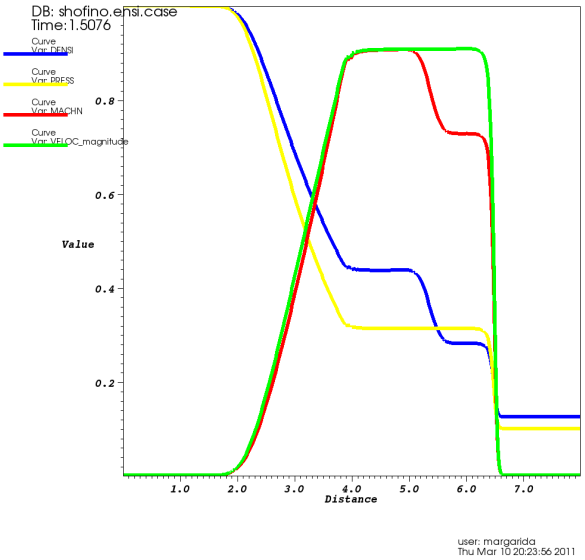


Figure 3: Sod's shock tube. Comparison of the solution of the density (blue line), pressure (yellow line), Mach number (red line), and velocity module (green line), using different number of frequencies and Gauss points for the Fourier subscale. The solution is advanced to $t \approx 1.5$.

(a) Diagonal $\tau$ subscale (b) Fourier subscale

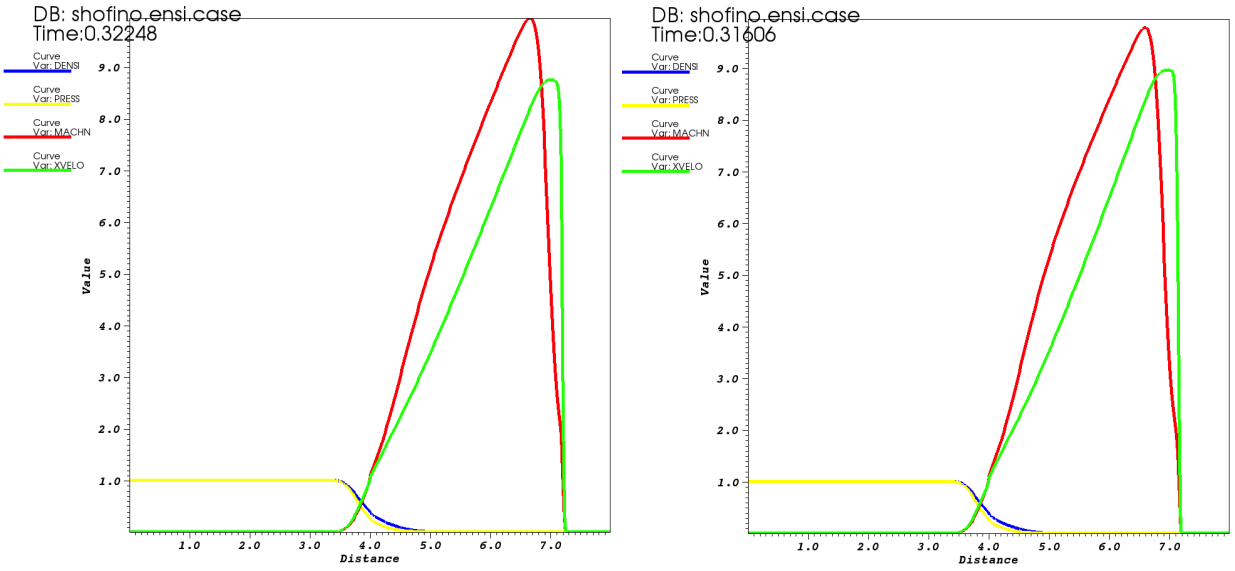


Figure 4: Sod's shock tube. We compare the diagonal $\tau$ and the Fourier subscale results of the density (blue line), pressure (yellow line), Mach number (red line), and velocity module (green line), for a supersonic case of the shock tube that reaches a maximum Mach number of around 10. We use a CFL number of 0.8, 4 Gauss integration points, and the Fourier subscale uses $M_{\text{freq}} = 1$.

### *4.2. Carter plate*

We solve the flow over the Carter plate [6, 39] which is a two-dimensional supersonic viscous flow that enters a rectangular region from its left side at a Mach number of 3 and a Reynolds number of 1000. This problem reaches a steady state. The surface of the domain is divided in two parts, the first part from $x_1 = -1$ to $x_1 = -0.8$ is a slip wall and the rest of the surface from $x_1 = -0.8$ to $x_1 = 1$ is the so-called plate that is non-slip. The initial conditions are $M = 3$, $\rho = 1$, $\mathbf{u} = (1, 0)$, $T = 0.00028$, $\mu = 0.001$, and $Pr = 0.72$. $c_{\text{p}}$, $c_{\text{v}}$, and $\kappa$ are determined to obtain the desired Mach and Prandtl numbers. We use in this problem the Sutherland viscosity law:

$$\frac{\mu}{\mu_{\text{ref}}} = \frac{T_{\text{ref}} + 110.3}{T + 110.3} \left( \frac{T}{T_{\text{ref}}} \right)^{\frac{3}{2}} , \tag{68}$$

where $\mu_{\text{ref}}$ and $T_{\text{ref}}$ are the inflow values of $\mu$ and $T$, respectively.

We impose the following boundary conditions. The non-slip boundary condition on the plate consists of setting $\mathbf{u} = 0$ and a stagnation temperature of $T = 0.00078$. A slip boundary condition

(a) Density and pressure

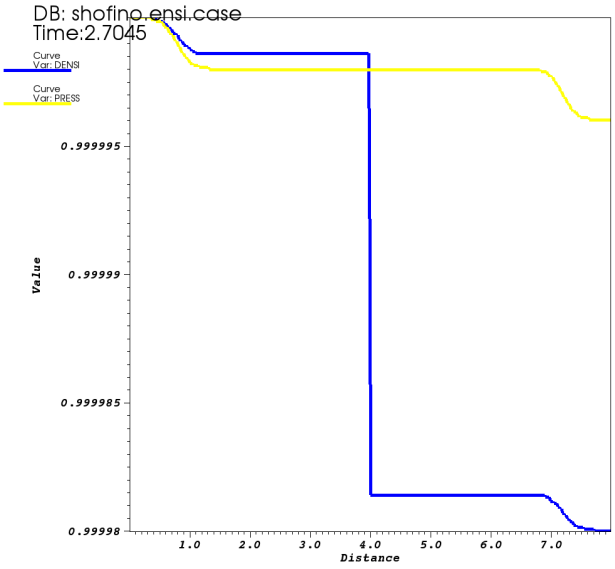


(b) Mach number and velocity module

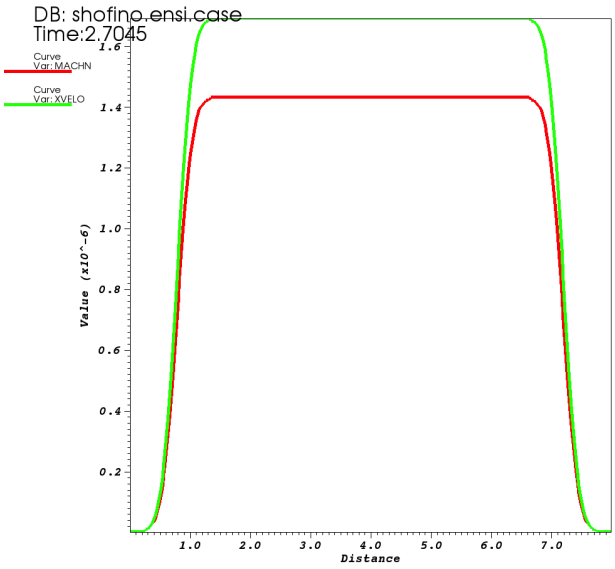


Figure 5: Sod's shock tube. Results for the diagonal $\tau$ subscale, of the density (blue line), pressure (yellow line), Mach number (red line), and velocity module (green line), for a very subsonic case of the shock tube that reaches a maximum Mach number of around $1.4 \times 10^{-6}$. We use a CFL number of 0.8 and 4 Gauss integration points. The corresponding results for the Fourier subscale using $M_{\text{freq}} = 1$, are not shown here because they are almost identical to the diagonal $\tau$ subscale ones.

is imposed on the first section of the surface as well as on the top wall, that is we impose $u_2 = 0$. Velocity $\mathbf{u}$, density $\rho$, and temperature $T$ are imposed on the inflow boundary at the same values as for the initial conditions and the outflow is left free of boundary conditions. We solve this problem using a structured mesh of 27000 rectangles and 27336 nodes.

To avoid spurious oscillations around the shocks a discontinuity capturing diffusion is required. Isotropic shock capturing (62) is used in this problem. This case is solved using a CFL number of 0.6, 4 integration Gauss points, and $M_{\text{freq}} = 2$ for the Fourier subscale. We consider that convergence is achieved when the total residual is of the order of $10^{-4}$.

When the supersonic flow enters the region, a curved shock and a boundary layer are developed from the leading edge of the plate. The shock is formed due to the big inflow velocity and the changing boundary condition on the surface. This can be seen on the contours of the Mach number

once the steady solution is reached, which are presented in Fig. 6. We observe that the diagonal $\tau$ subscale and the Fourier subscale give very similar result. This fact is also seen from Fig. 7, where we compare the Mach number result over a vertical line passing by $x_1 = 0$, for the two subscale options. It is observed that our results are in good agreement with those presented in the literature: [6, 36, 18].

(a) Diagonal $\tau$ subscale

(b) Fourier subscale

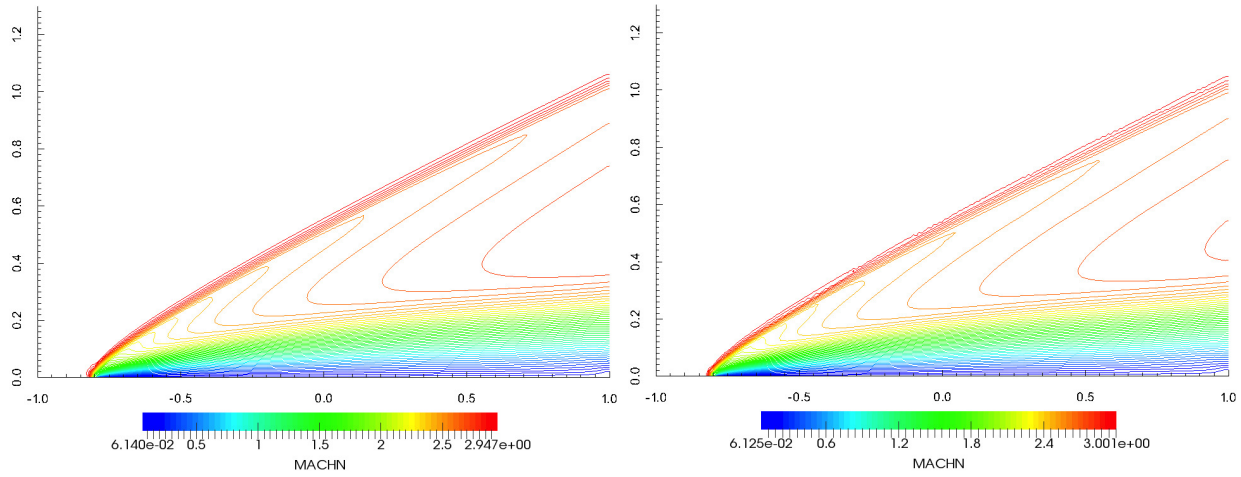


Figure 6: Carter's problem. Mach number contours corresponding to the diagonal $\tau$ subscale and the Fourier subscale. We use 4 Gauss points and the isotropic shock capturing for these simulations. The Fourier subscale uses $M_{\text{freq}} = 2$.

### *4.3. Scramjet*

We solve the two-dimensional inviscid flow past a supersonic scramjet inlet configuration having two struts [40, 41, 42]. This problem reaches a steady state. The initial conditions are: the Mach number $M = 5$, the velocity $\mathbf{u} = (1, 0)$, the density $\rho = 1$, and the temperature $T = 1$. $c_{\text{p}}$ and $c_{\text{v}}$ are determined to obtain the desired Mach number. The boundary conditions consist of imposing the velocity, the density, and the temperature at the inflow and the outflow is set free. The normal velocity is imposed to be zero on the surface wall, the top wall, and the two struts boundaries. We use an unstructured mesh of 95103 triangles and 48535 nodal points. Anisotropic shock capturing (62) is required for this simulation, otherwise the solution blows-up. This case is solved using a CFL number of 0.6, 3 integration Gauss points, and $M_{\text{freq}} = 2$ for the Fourier subscale. We consider

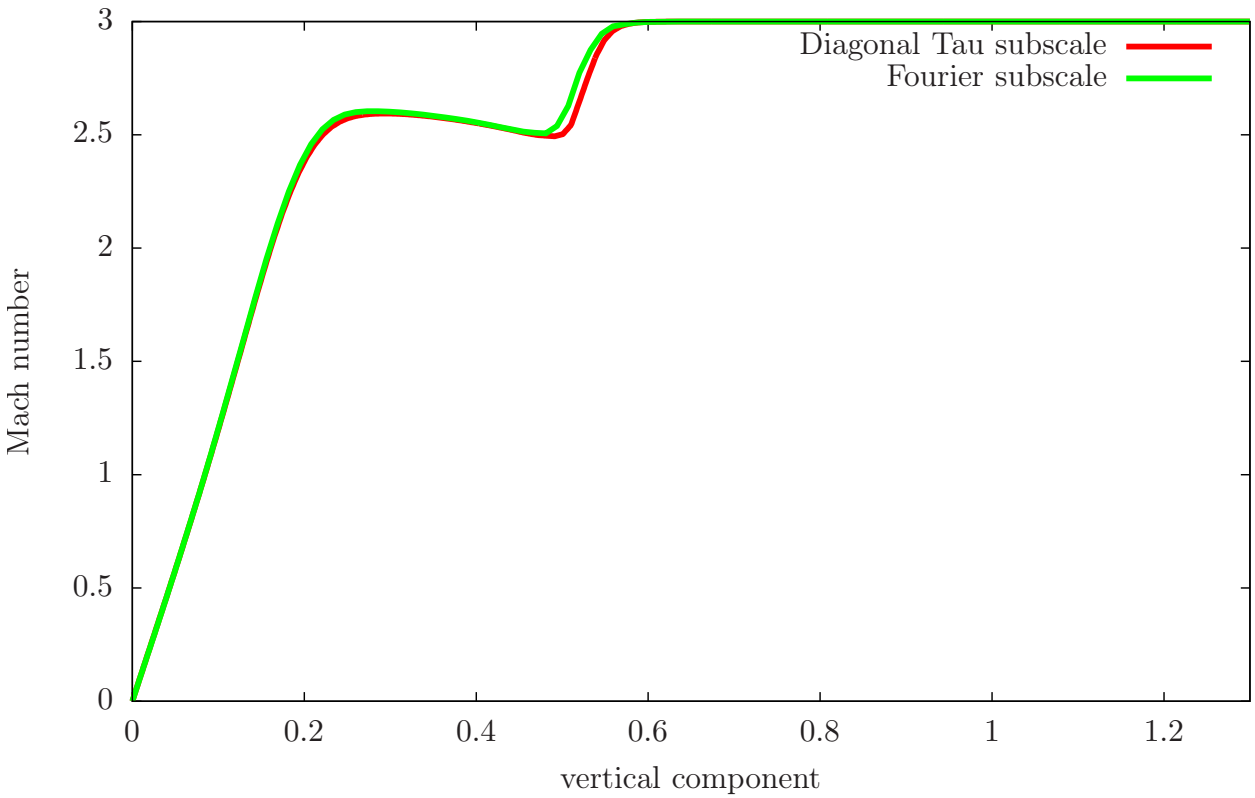


Figure 7: Carter's problem. Comparison of the diagonal $\tau$ subscale (red line) and the Fourier subscale (green line) results for the Mach number over a vertical line of the domain passing by $x_1 = 0$. We use 4 Gauss points and the isotropic shock capturing for these simulations. The Fourier subscale uses $M_{\text{freq}} = 2$.

that convergence is achieved when the total residual is of the order of $10^{-5}$.

In Fig. 8 we compare pressure and Mach number contours for the diagonal $\tau$ subscale and the Fourier subscale. We observe that the shocks are placed at the same location for both options, however the diagonal $\tau$ subscale option give a slightly smoother solution. In Fig. 9 we show for the diagonal $\tau$ subscale option the result of the Mach contours over two embedded meshes, the original one of 95103 elements and 48535 grid points, and a refined one having 380412 elements and 192200 grid points. We can appreciate that the shocks are sharper on the fine mesh but its placement is the same in both meshes. Compared with [41] our results are less oscillatory and the shocks are more sharply captured.

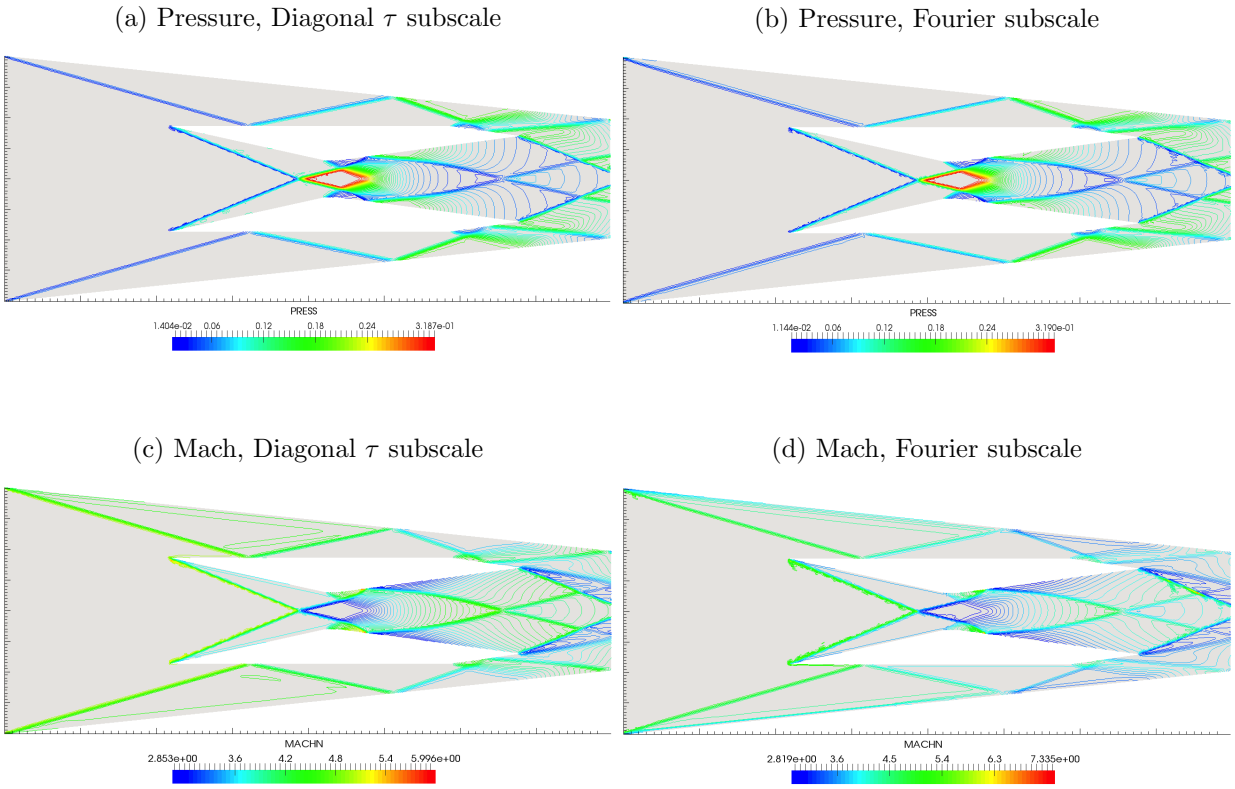


Figure 8: Scramjet problem. Scramjet contours for the pressure and the Mach number using anisotropic shock capturing and 3 Gauss points. The diagonal $\tau$ subscale and the Fourier subscale results are displayed for comparison. The Fourier subscale uses $M_{\text{freq}} = 2$.

## 5. Conclusions

We introduced a variational multiscale stabilization method for compressible flows. Two different options are presented for the modeling of the subscales: 1) the diagonal $\tau$ subscale and 2) the Fourier subscale. Their results are compared on several two-dimensional test cases, for viscous and inviscid, steady and transient flows at different Mach numbers, from subsonic to supersonic regimes. The first option for the subscale presents a simpler structure, involves less computational cost, and gives similar results compared to the second option. For this reason, for the time being we conclude that a variational multiscale stabilization based on the diagonal $\tau$ subscale is more convenient. However further research on the Fourier subscale should be carried on with the purpose of simplifying and improving it. A variational multiscale stabilization based on the diagonal

(a) Original mesh (b) Refined mesh

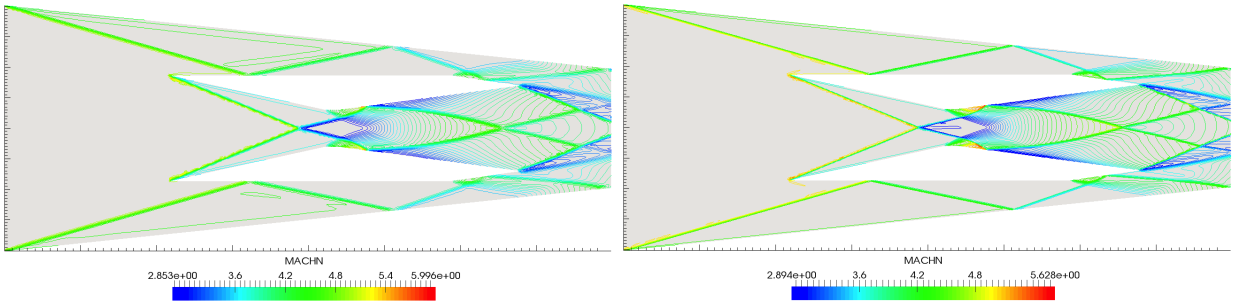


Figure 9: Scramjet problem. Contours of the Mach number for the diagonal $\tau$ subscale using the original mesh of 95103 elements and a refined embedded mesh of 380412 elements.

tau subscale has been adopted, coupled to local preconditioning techniques, and tested further on three dimensional cases in [23, 24, 25].

## 6. Acknowledgments

This research is supported at BCAM by the Basque Government under Grants ICERMAR KK-2015/00097 and ICERMAR 2 KK-2016/100031 and also through the BERC 2014-2017 program and by Spanish Ministry of Economy and Competitiveness MINECO: BCAM Severo Ochoa excellence accreditation SEV-2013- 0323.

## Appendix A. Jacobian and diffusion matrices

The jacobian matrices $\mathbf{A}^i(\mathbf{\Phi})$, for $i = 1, \ldots, 3$, read

$$\mathbf{A}^1(\mathbf{\Phi}) = \begin{pmatrix} (2 - \frac{R}{c_v})\frac{U_1}{\rho} & -\frac{R}{c_v}\frac{U_2}{\rho} & -\frac{R}{c_v}\frac{U_3}{\rho} & -\frac{U_1^2}{\rho^2} + \frac{1}{2}\frac{R}{c_v}\frac{U_k U_k}{\rho^2} & \frac{R}{c_v} \\ \frac{U_2}{\rho} & \frac{U_1}{\rho} & 0 & -\frac{U_1 U_2}{\rho^2} & 0 \\ \frac{U_3}{\rho} & 0 & \frac{U_1}{\rho} & -\frac{U_1 U_3}{\rho^2} & 0 \\ 1 & 0 & 0 & 0 & 0 \\ \frac{1}{\rho}(E + p - \frac{R}{c_v}\frac{U_1^2}{\rho}) & \frac{-R}{c_v}\frac{U_1 U_2}{\rho^2} & \frac{-R}{c_v}\frac{U_1 U_3}{\rho^2} & \frac{-U_1}{\rho^2}(E + p - \frac{1}{2}\frac{R}{c_v}\frac{U_k U_k}{\rho}) & (1 + \frac{R}{c_v})\frac{U_1}{\rho} \end{pmatrix}, \tag{A.1}$$

$$\mathbf{A}^2(\mathbf{\Phi}) = \begin{pmatrix} \frac{U_2}{\rho} & \frac{U_1}{\rho} & 0 & -\frac{U_2 U_1}{\rho^2} & 0 \\ -\frac{R}{c_v}\frac{U_1}{\rho} & (2 - \frac{R}{c_v})\frac{U_2}{\rho} & -\frac{R}{c_v}\frac{U_3}{\rho} & -\frac{U_2^2}{\rho^2} + \frac{1}{2}\frac{R}{c_v}\frac{U_k U_k}{\rho^2} & \frac{R}{c_v} \\ 0 & \frac{U_3}{\rho} & \frac{U_2}{\rho} & -\frac{U_2 U_3}{\rho^2} & 0 \\ 0 & 1 & 0 & 0 & 0 \\ \frac{-R}{c_v}\frac{U_2 U_1}{\rho^2} & \frac{1}{\rho}(E + p - \frac{R}{c_v}\frac{U_2^2}{\rho}) & \frac{-R}{c_v}\frac{U_2 U_3}{\rho^2} & \frac{-U_2}{\rho^2}(E + p - \frac{1}{2}\frac{R}{c_v}\frac{U_k U_k}{\rho}) & (1 + \frac{R}{c_v})\frac{U_2}{\rho} \end{pmatrix}, \tag{A.2}$$

$$\mathbf{A}^3(\mathbf{\Phi}) = \begin{pmatrix} \frac{U_3}{\rho} & 0 & \frac{U_1}{\rho} & -\frac{U_3 U_1}{\rho^2} & 0 \\ 0 & \frac{U_3}{\rho} & \frac{U_2}{\rho} & -\frac{U_3 U_2}{\rho^2} & 0 \\ -\frac{R}{c_v}\frac{U_1}{\rho} & -\frac{R}{c_v}\frac{U_2}{\rho} & (2 - \frac{R}{c_v})\frac{U_3}{\rho} & -\frac{U_3^2}{\rho^2} + \frac{1}{2}\frac{R}{c_v}\frac{U_k U_k}{\rho^2} & \frac{R}{c_v} \\ 0 & 0 & 1 & 0 & 0 \\ \frac{-R}{c_v}\frac{U_3 U_1}{\rho^2} & \frac{-R}{c_v}\frac{U_3 U_2}{\rho^2} & \frac{1}{\rho}(E + p - \frac{R}{c_v}\frac{U_3^2}{\rho}) & \frac{-U_3}{\rho^2}(E + p - \frac{1}{2}\frac{R}{c_v}\frac{U_k U_k}{\rho}) & (1 + \frac{R}{c_v})\frac{U_3}{\rho} \end{pmatrix}. \tag{A.3}$$

The diffusion matrices $\mathbf{K}^{ir}$, for $i, r = 1, \ldots, 3$, read

$$\mathbf{K}^{ir}(\mathbf{\Phi})_{kl} = \begin{cases} (\delta_{kl}\delta_{ir} + \delta_{il}\delta_{kr} - \frac{2}{3}\delta_{ki}\delta_{rl})\frac{\mu}{\rho} & k,\, l = 1, \ldots, 3 \\ -\delta_{kr}\frac{\mu U_i}{\rho^2} - \delta_{ri}\frac{\mu U_k}{\rho^2} + \frac{2}{3}\delta_{ki}\frac{\mu U_r}{\rho^2} & k = 1, \ldots, 3,\, l = 4 \\ 0 & k = 1, \ldots, 3,\, l = 5 \\ 0 & k = 4,\, l = 1, \ldots, 5 \\ \delta_{ir}\frac{(\mu - \frac{\kappa}{c_v})U_l}{\rho^2} + \delta_{il}\frac{\mu U_r}{\rho^2} - \frac{2}{3}\delta_{rl}\frac{\mu U_i}{\rho^2} & k = 5,\, l = 1, \ldots, 3 \\ \frac{1}{2}\frac{\mu U_i U_r}{\rho^3} - \delta_{ir}(\frac{(\mu - \frac{k}{c_v})\|\mathbf{U}\|^2}{\rho^3} + \frac{\kappa}{c_v}\frac{E}{\rho^2}) & k = 5,\, l = 4 \\ \delta_{ir}\frac{1}{\rho}\frac{\kappa}{c_v} & k = 5,\, l = 5 \end{cases} \tag{A.4}$$

[1] A. Quarteroni, A. Valli, Numerical Approximation of Partial Differential Equations, Springer, 1994.

[2] T. J. R. Hughes, T. Tezduyar, Finite element methods for first-order hyperbolic systems with particular emphasis on the compressible Euler equations, Comput. Methods Appl. Mech. Engrg. 45 (1984) 217–284.

[3] T. J. R. Hughes, M. Mallet, A new finite element formulation for computational fluid dynamics: III. The generalized streamline operator for multidimensional advective-diffusive systems, Comp. Methods Appl. Mech. Engrg. 58 (1986) 305–328.

[4] G. J. Le Beau, S. E. Ray, S. K. Aliabadi, T. E. Tezduyar, SUPG finite element computation of compressible flows with the entropy and conservation variables formulations, Comp. Methods Appl. Mech. Engrg. 104 (1993) 397–422.

[5] T. E. Tezduyar, M. Senga, Stabilization and shock-capturing parameters in SUPG formulation of compressible flows, Computer Methods in Applied Mechanics and Engineering 195 (13-16) (2006) 1621 – 1632, a Tribute to Thomas J.R. Hughes on the Occasion of his 60th Birthday. doi:http://dx.doi.org/10.1016/j.cma.2005.05.032.
URL http://www.sciencedirect.com/science/article/pii/S0045782505002999

[6] F. Shakib, T. J. R. Hughes, Z. Johan, A new finite element formulation for computational fluid dynamics: X. The compressible Euler and Navier-Stokes equations, Comput. Methods Appl. Mech. Engrg. 89 (1991) 141–291.

[7] T. Hughes, G. Scovazzi, T. E. Tezduyar, Stabilized methods for compressible flows, J. Sci. Comput. 43 (2010) 343–368.

[8] T. Hughes, Multiscale phenomena: Green's functions, the Dirichlet-to-Neumann formulation, subgrid scale models, bubbles and the origins of stabilized methods, Comput. Methods Appl. Mech. and Engrg. 127 (1995) 387–401.

[9] T. J. R. Hughes, G. Feijoo, L. Mazzei, J. Quincy, The variational multiscale method – A paradigm for computational mechanics, Comput. Methods Appl. Mech. Engrg. 166 (1998) 3–24.

[10] R. Codina, J. Blasco, Analysis of a stabilized finite element approximation of the transient convection-diffusion-reaction equation using orthogonal subscales, Comput. Visusl. Sci. 4 (2002) 167–174.

[11] A. Corsini, F. Rispoli, A. Santoriello, A variational multiscale higher-order finite element formulation for turbomachinery flow computations, Computer Methods in Applied Mechanics and Engineering 194 (45-47) (2005) 4797–4823. doi:10.1016/j.cma.2004.11.013.
URL http://www.sciencedirect.com/science/article/pii/S004578250400564X

[12] G. Houzeaux, B. Eguzkitza, M. Vázquez, A variational multiscale model for the advection-diffusion-reaction equation, Comm. Numer. Meth. Engrg. 25 (2009) 787–809.

[13] T. J. R. Hughes, L. Mazzei, K. E. Jansen, Large Eddy Simulation and the variational multiscale method, Comput. Visual. Sci. 3 (2000) 47–59.

[14] R. Codina, Stabilized finite element approximation of transient incompressible flows using orthogonal subscales, Comput. Methods Appl. Mech. Engrg. 191 (2002) 4295–4321.

[15] V. Gravemeier, The variational multiscale method for laminar and turbulent incompressible flow, Ph.D. thesis, Universitat Stuttgart (2003).

[16] Y. Bazilevs, V. Calo, J. A. Cottrell, T. J. R. Hughes, A. Reali, G. Scovazzi, Variational multiscale residual-based turbulence modeling for large eddy simulation of incompressible flows, Comput. Methods Appl. Mech. Engrg.

197 (2007) 173–201.

[17] M. Avila, R. Codina, J. Principe, Large eddy simulation of low mach number flows using dynamic and orthogonal subgrid scales, Comput. Fluids 99 (2014) 44–66.

[18] F. Rispoli, R. Saavedra, A stabilized finite element method based on SGS models for compressible flows, Comput. Methods Appl. Mech. and Engrg. 196 (2006) 652–664.

[19] F. Rispoli, R. Saavedra, A. Corsini, T. E. Tezduyar, Computation of inviscid compressible flow with V-SGS stabilization and $YZ\beta$ shock capturing, Int. J. Numer. Methods Fluids 54 (2007) 695–706.

[20] S. Marras, M. Moragues, M. Vázquez, O. Jorba, G. Houzeaux, A variational multiscale stabilized finite element method for the solution of the Euler equations of nonhydrostatic stratified flows, Journal of Computational Physics 236 (2013) 380 – 407. doi:http://dx.doi.org/10.1016/j.jcp.2013.06.006.

[21] S. Marras, M. Moragues, M. Vázquez, O. Jorba, G. Houzeaux, Simulations of moist convection by a variational multiscale stabilized finite element method, Journal of Computational Physics 252 (2013) 195 – 218. doi:http://dx.doi.org/10.1016/j.jcp.2013.06.006.

[22] S. Marras, J. F. Kelly, M. Moragues, A. Müller, M. A. Kopera, M. Vázquez, F. X. Giraldo, G. Houzeaux, O. Jorba, A review of element-based Galerkin methods for numerical weather prediction: Finite elements, spectral elements, and discontinuous Galerkin, Archives of Computational Methods in Engineering (2015) 1–50doi:10.1007/s11831-015-9152-1.
URL http://dx.doi.org/10.1007/s11831-015-9152-1

[23] M. Moragues, M. Vázquez, G. Houzeaux, Local preconditioning and variational multiscale stabilization for Euler compressible steady flow, Computer Methods in Applied Mechanics and Engineering 305 (2016) 468 – 500. doi:https://doi.org/10.1016/j.cma.2016.02.027.
URL http://www.sciencedirect.com/science/article/pii/S0045782516300573

[24] M. Moragues, G. Bernardino, M. Vázquez, G. Houzeaux, Fourier stability analysis and local Courant number of the preconditioned variational multiscale stabilization (P-VMS) for Euler compressible flow, Computer Methods in Applied Mechanics and Engineering 301 (2016) 28 – 51. doi:http://dx.doi.org/10.1016/j.cma.2015.12.008.
URL http://www.sciencedirect.com/science/article/pii/S0045782515004107

[25] M. Moragues Ginard, Variational multiscale stabilization and local preconditioning for compressible flow, Ph.D. thesis, Universitat Politècnica de Catalunya, Barcelona, Spain (2016).

[26] S. S. Collis, Y. Chang, The DG/VMS method for unified turbulence simulation, AIAA paper 3124 (2002) 24–27.

[27] B. Koobus, F. Charbel, A variational multiscale method for the large eddy simulation of compressible turbulent flows on unstructured meshes - application to vortex shedding, Comp. Methods Appl. Mech. Engr. 193 (2004) 1367–1383.

[28] C. Farhat, A. K. Rajasekharan, B. Koobus, A dynamic variational multiscale method for large eddy simulations on unstructured meshes, Computer Methods in Applied Mechanics and Engineering 195 (13-16) (2006) 1667 – 1691, a Tribute to Thomas J.R. Hughes on the Occasion of his 60th Birthday. doi:http://dx.doi.org/10.1016/j.cma.2005.05.045.
URL http://www.sciencedirect.com/science/article/pii/S0045782505003014

[29] H. Ouvrard, B. Koobus, A. Dervieux, M. V. Salvetti, Classical and variational multiscale LES of the

flow around a circular cylinder on unstructured grids, Computers & Fluids 39 (7) (2010) 1083 – 1094. doi:http://dx.doi.org/10.1016/j.compfluid.2010.01.017.
URL http://www.sciencedirect.com/science/article/pii/S0045793010000319

[30] V. Levasseur, P. Sagaut, F. Chalot, A. Davroux, An entropy-variable-based VMS/GLS method for the simulation of compressible flows on unstructured grids, Computer Methods in Applied Mechanics and Engineering 195 (9-12) (2006) 1154 – 1179. doi:http://dx.doi.org/10.1016/j.cma.2005.04.009.
URL http://www.sciencedirect.com/science/article/pii/S0045782505001568

[31] F. van der Bos, J. J. van der Vegt, B. J. Geurts, A multiscale formulation for compressible turbulent flow suitable for general variational discretization techniques, Comput. Methods Appl. Mech. Engrg. 196 (2007) 2863–2875.

[32] V. John, P. Knobloch, On spurious oscillations at layers diminishing (SOLD) methods for convection-diffusion equations: Part I - A review, Comput. Methods Appl. Mech. Engrg. 196 (2007) 2197–2215.

[33] R. Leveque, Finite volume methods for hyperbolic problems, 1st Edition, Cambridge University Press, 2002.

[34] R. Courant, K. Friedrichs, H. Lewy, On the partial difference equations of mathematical physics, IBM Journal Res. Dev. 11 (2) (1967) 215–234.

[35] T. R. Hughes, The finite element method: Linear static and dynamic finite element analysis, 2nd Edition, Dover Publications Inc., 2000.

[36] M. Vázquez, Numerical modeling of compressible laminar and turbulent flow: the characteristic based split (CBS) finite element general algorithm, Ph.D. thesis, Universitat Politècnica de Catalunya, Barcelona, Spain (1998).

[37] R. Codina, A discontinuity-capturing crosswind-dissipation for the finite element solution of the convection-diffusion equation, Comput. Methods Appl. Mech. and Engrg. 110 (1993) 325–342.

[38] G. A. Sod, A survey of several finite difference methods for systems of nonlinear hyperbolic conservation laws, Journal of Computational Physics 27 (1) (1978) 1–31.

[39] O. Zienkiewicz, K. Morgan, B. Satya Say, R. Codina, M. Vázquez, A general algorithm for compressible and incompressible flow - Part II. Tests on the explicit form, Int. J. Numer. Meth. Fluids 20 (1995) 887–913.

[40] A. Kumar, Numerical analysis of the scramjet inlet flow field using two-dimensional Navier-Stokes equations, in: Proceedings: 19th AIAA Aerospace Sciences Meeting, St. Louis, Missouri, 1981.

[41] A. Kumar, Two-dimensional analysis of a scramjet inlet flowfield, AIAA Journal 20 (1) (1982) 96–97.

[42] A. Kumar, S. N. Tiwari, Analysis of the scramjet inlet flow field using two-dimensional Navier-Stokes equations, Tech. Rep. 3562, NASA (1982).